MOLECULAR SEPARATION

Discrimination of xylene isomers in a stacked coordination polymer

Liangying Li[1,2]†, Lidong Guo[1]†, David H. Olson[2], Shikai Xian[2,3], Zhiguo Zhang[1,4], Qiwei Yang[1,4], Kaiyi Wu[1], Yiwen Yang[1,4], Zongbi Bao[1,4]*, Qilong Ren[1,4], Jing Li[2,3]*

The separation and purification of xylene isomers is an industrially important but challenging process. Developing highly efficient adsorbents is crucial for the implementation of simulated moving bed technology for industrial separation of these isomers. Herein, we report a stacked one-dimensional coordination polymer {[Mn(dhbq)(H_2O)$_2$], H_2dhbq = 2,5-dihydroxy-1,4-benzoquinone} that exhibits an ideal molecular recognition and sieving of xylene isomers. Its distinct temperature-adsorbate–dependent adsorption behavior enables full separation of *p*-, *m*-, and *o*-xylene isomers in both vapor and liquid phases. The delicate stimuli-responsive swelling of the structure imparts this porous material with exceptionally high flexibility and stability, well-balanced adsorption capacity, high selectivity, and fast kinetics at conditions mimicking industrial settings. This study may offer an alternative approach for energy-efficient and adsorption-based industrial xylene separation and purification processes.

Xylene isomers are widely used as raw chemicals for manufacturing large-scale industrial commodities (*1*, *2*). Separation of xylene isomers through distillation is an energy-intensive process because of their nearly-the-same boiling points (table S1) (*3*). The dominant industrial method for large-scale separation of xylene isomers is based on simulated moving bed (SMB) using FAU-type zeolites as the stationary phase (*4*), which is favorably run at relatively high temperatures (393 to 523 K or 120° to 250°C) to ensure a sufficient mass-transfer rate and to reduce viscosity of the mobile phase as well as pressure drop across adsorbent beds connected in a series (*4*, *5*). However, these zeolite adsorbents suffer from low selectivity and/or uptake capacity as a result of limited porosity, structural tunability, and high rigidity (*6*). Therefore, developing stable and high-performance adsorbents represents an important current interest for the efficient separation of xylene isomers.

Solid adsorbents, such as MFI-type zeolites (*7*), molecular crystals (*8*–*10*), metal complexes (*11*, *12*), organic cages (*13*), and metal-organic frameworks (MOFs) (*14*–*20*), have been investigated for the separation of xylene isomers. A particular feature of dynamic MOFs is their framework flexibility, which has led to interesting and unexpected adsorption properties (*21*–*24*). Such structural flexibility, including breathing and gate-opening (Fig. 1A), has been utilized for the selective adsorption of xylenes (*25*–*28*); however, a complete separation of all three isomers by molecular recognition or sieving has not yet been realized.

We report a manganese-based stacked one-dimensional (1D) coordination polymer, Mn(dhbq)(H_2O)$_2$ (Mn-dhbq, H_2dhbq = 2,5-dihydroxy-1,4-benzoquinone), and its performance for discrimination and separation of xylene isomers in the temperature range of 303 to 393 K (30° to ~120°C). Mn-dhbq exhibits distinct changes in the interchain distances when exposed to xylene molecules, leading to a framework swelling (Fig. 1A) and discriminative adsorption behavior toward the three isomers.

Mn-dhbq was obtained as a brown-orange–colored microcrystalline solid (fig. S1), following the reported procedure with minor modifications (*29*, *30*). The structure of the as-synthesized Mn-dhbq was refined by Rietveld method using the room-temperature powder x-ray diffraction (PXRD) data (fig. S2), which are in good agreement with those reported by Kitagawa (table S3) (*29*, *30*). Each dhbq coordinates to two Mn^{2+} (Fig. 1B), and each Mn^{2+} bonds to four oxygens from two ligands and two oxygens from two coordinated water molecules, resulting in a strip-like 1D straight chain (Fig. 1C). The adjacent chains are linked by multiple hydrogen bonds, leading to a H-bonded 3D network with a hydrogen bond distance of 1.754 Å (Fig. 1, C and D). Upon activation, coordinated water molecules were removed, and the sample remained stable up to 748 K (475°C) (fig. S3), confirmed by the porosity analysis (fig. S4). The framework underwent a structure transformation accompanied by color change (fig. S5). This structural change is reversible (figs. S6 and S7). The Brunauer-Emmett-Teller (BET) surface area was estimated to be ~429 m^2/g with a pore size of ~5.6 Å (table S4). Based on Connolly surface and pore analysis by Material Studio 2017R2 (Accelrys Software, Inc.) using the as-made structure (with water molecules removed), the isolated tubular-shaped voids (Fig. 1, E and F) would be too small to hold xylene molecules. In reality, however, the activated Mn-dhbq shows strong adsorption toward xylenes, which suggests an expansion of pore space.

Single-component vapor adsorption isotherms of xylene isomers were collected at 303, 333, 363, and 393 K on Mn-dhbq powder samples. Molecular sieving–based full separation of xylene isomers was achieved with the affinity following the trend of para-xylene (PX) > meta-xylene (MX) > ortho-xylene (OX). At 333 K, the compound adsorbs both PX and MX but almost fully excludes OX (Fig. 2A). The uptake capacities are 185, 159, and 23 mg/g for PX, MX, and OX, respectively, at 1.05 kPa. This result reveals that OX can be sieved out at this temperature. At a higher temperature (393 K), both MX and OX are essentially excluded, with uptake capacities of 141, 17, and 22 mg/g, respectively, for PX, MX, and OX at 1.05 kPa (fig. S13). For effective separations, adsorption capacity is an equally important parameter as selectivity. Mn-dhbq takes up substantially higher amounts of PX than those of best-performing PX-selective adsorbents. For example, the maximum uptake amounts of MFI zeolite (131.4 mg/g, 298 K) (*7*), Zn-MOF (55 mg/g, 298 K) (*27*), and Cu-metallocycle (140 mg/g, 293 K) (*12*) are all considerably lower than that of Mn-dhbq (>200 mg/g) measured at a higher temperature (303 K). The temperature-dependent adsorption behavior of Mn-dhbq allows for separation of both PX/OX and PX/MX binary mixtures. Notably, the adsorption isotherms of PX exhibit steep slopes, reaching saturation at very low pressure, which suggests strong interactions of Mn-dhbq with PX. Distinct inflection points were observed in both MX and OX isotherms (figs. S10 to S13)—an indication of swelling of the Mn-dhbq structure in response to the external stimulus. The adsorption performance was retained for the formulated pellet samples (Fig. 2D and figs. S8, S9, and S14 to S16).

To assess the capability of Mn-dhbq for selective recognition of a specific xylene, we performed competitive adsorption measurements on xylene mixtures in both vapor and liquid phase. The data were analyzed by proton nuclear magnetic resonance (^{1}H-NMR) (Fig. 2B and figs. S17 to S28) and gas chromatography (figs. S29 to S32). For equimolar binary vapor mixtures, the relative adsorption selectivities of Mn-dhbq are 34.8/1 and 37.9/1 for PX/MX and PX/OX at 363 K, respectively (figs. S24 and S25), and 12.5/1 for MX/OX at 333 K (fig. S26). These values are higher than most previously reported numbers (Fig. 2E and table S2). Additionally, a high selectivity of 70.4/2.5/1 was obtained for an equimolar ternary vapor mixture of PX/MX/OX at 363 K (fig. S28). The

[1]Key Laboratory of Biomass Chemical Engineering of Ministry of Education, College of Chemical and Biological Engineering, Zhejiang University, Hangzhou 310027, P. R. China. [2]Department of Chemistry and Chemical Biology, Rutgers University, Piscataway, NJ 08854, USA. [3]Hoffmann Institute of Advanced Materials, Shenzhen Polytechnic, Shenzhen 518055, P. R. China. [4]Institute of Zhejiang University-Quzhou, Quzhou 324000, P. R. China.
*Corresponding author. Email: baozb@zju.edu.cn (Z.B.); jingli@rutgers.edu (J.L.)
†These authors contributed equally to this work.

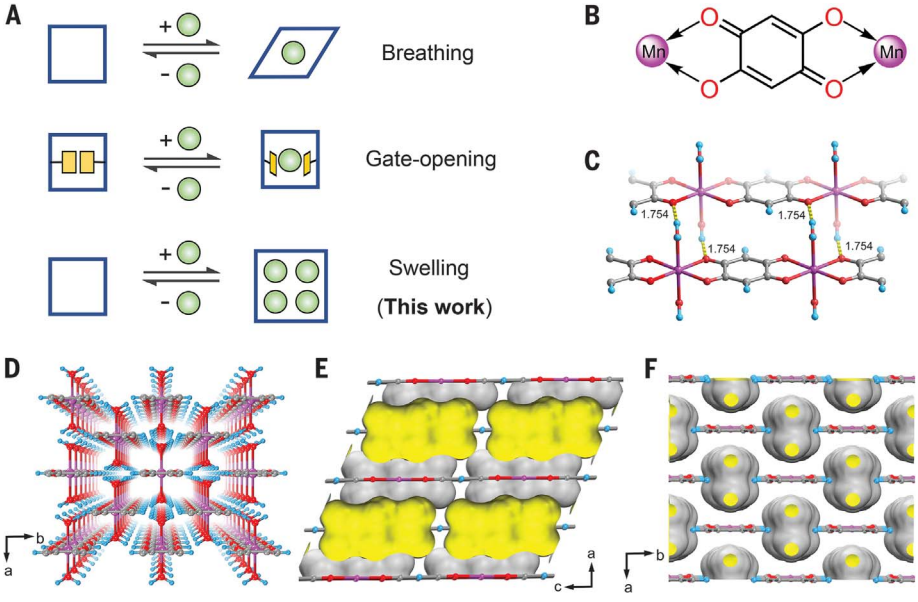

Fig. 1. The structure and pore properties of Mn-dhbq. (**A**) Representations of different modes of framework dynamics or flexibility: breathing, gate opening-closing or linker rotation, and swelling. (**B**) The coordination mode of the dhbq linker. (**C**) The hydrogen bonds between the two adjacent 1D chains within the framework (yellow dashed lines). (**D**) Perspective view of the crystal structure of as-synthesized Mn-dhbq along the *c* axis. (**E** and **F**) The pore spaces within the Mn-dhbq structure without the coordinated water molecules. The unit cell is kept the same as the as-synthesized structure. The pore sizes in both (E) and (F) are too small to allow xylene molecules to be adsorbed.

adsorbed amount of PX was slightly affected by the presence MX and OX, with the uptake decreased from 159 mg/g (single component) to 140 mg/g (ternary mixture) at 363 K.

Furthermore, we carried out static solid-liquid extraction experiments at temperatures between 303 and 393 K to evaluate separation performance in liquid phase. The results confirmed the distinct selectivities of Mn-dhbq in the order of PX >> MX >> OX, especially at the higher temperatures necessary to meet the mass-transfer rate requirement for industrial SMB processes. It is worth noting that although Cu-metallocycle demonstrates impressive selectivity at lower temperatures, the value continues to drop quickly as temperature increases (table S5 and figs. S33 to S36). At 363 and 393 K, its selectivity for ternary mixture PX/OX/MX (45.4/1.4/1 and 19.4/1.6/1) becomes substantially lower than that of Mn-dhbq (78.4/3.8/1 and 84.6/2.5/1). Notably, Mn-dhbq preferentially adsorbs PX from a quaternary liquid mixture (PX/OX/MX/EB = 22/22/50/6) at a composition identical to that used in a licensed UOP (Honeywell UOP, formerly known as UOP LLC or Universal Oil Products) Parex process (*31*). Its selectivity (171.1/4.9/1/18.4) is substantially higher than that of the Cu-metallocycle (86.6/3.3/1/6.6) at 393 K (figs. S31, S32, S35, and S36).

To evaluate the feasibility of Mn-dhbq for xylene separations under real-world conditions, breakthrough experiments were also conducted on pellet samples for vapor-phase binary and ternary xylene mixtures (figs. S37 to S40). The results are in excellent agreement with the trend determined from the pure-component vapor adsorption isotherms. At 363 K, PX can be fully separated from the PX/MX/OX ternary mixture, followed by a complete separation of MX from the binary mixture of MX/OX at 303 K (Fig. 2, C and F), which confirms that Mn-dhbq is the first adsorbent capable of full discrimination of the three xylene isomers in the vapor phase by molecular sieving mechanism.

High diffusion rates drastically decrease the adsorption-desorption time, which is crucial for industrial applications (*32*). In this regard, operation at elevated temperature is necessary to achieve fast kinetics and sufficient diffusion rate for practical separations of xylene mixtures. Adsorption kinetics experiments were performed to verify the mass-transfer rate of xylenes in Mn-dhbq using both gravimetric and volumetric methods, and time-dependent adsorption profiles of PX were measured between 303 and 393 K (figs. S41 to S46). The diffusion rate constant (D_c/r^2, per second) of PX in Mn-bhdq was obtained by fitting the kinetic curves according to Crank theory (*33*). The estimated values are 7.8×10^{-4} and 7.0×10^{-3} at 303 and 393 K, respectively (fig. S45), which outperform both BaX zeolite (4.8×10^{-3} at 453 K) (*34*) and Cu-metallocycle (7.6×10^{-5} and 4.5×10^{-4} at 303 and 393 K, respectively; fig. S46).

A detailed structural analysis of xylene-adsorbed Mn-dhbq was made using several techniques and methods. Although the samples remained crystalline, the broad PXRD peaks suggest high-level local disorders (figs. S47 to S50), making it difficult to solve their crystal structures. We also attempted to use the 3D microcrystal electron diffraction (micro-ED) method to reconstruct the structure, but without success (figs. S51 and S52). Nevertheless, because the 1D chains within the structure are not connected to each other by chemical bonds, but are only held together by weak interchain hydrogen bonds and/or van der Waals forces, the structure is highly flexible and can undergo a swelling to provide optimal constrained spaces for selective adsorption of xylene isomers (Fig. 3A). The large shifts in the (001), (100), and (020) diffraction planes of xylene-adsorbed Mn-dhbq from those of the as-synthesized and activated Mn-dhbq correlate to an increase in the interchain distance from 6.35 and 6.15 to 6.47 Å (Fig. 3C). The activated Mn-dhbq framework contains stacks of flexible 1D chains with a high concentration of open metal sites, offering favorable and size-specific adsorption binding sites between the chains.

Having the largest length (z) to width (x) ratio (1.38; table S1), PX fits very well in the space between the neighboring chains because of its similar geometry to the Mn-ligand-Mn segment, giving rise to strong affinity to Mn-dhbq (Fig. 3, B and E), consistent with the high uptake of PX of 208.4 mg/g at 303 K. OX, however, with the smallest z/x ratio (1.08; table S1), does not match well with the constrained space (Fig. 3, B and G) and thus has the least interaction with the chain. The interaction of MX with Mn-dhbq falls between that of PX and OX, in trend with its intermediate z/x ratio (1.23; table S1 and Fig. 3, B and F). The density functional theory (DFT) simulations provide a more quantitative assessment of the sorbate-sorbent interactions, illustrating that there are three different binding sites for xylene molecules. All three xylene molecules have comparable arene π-π stacking interactions (site I, green dotted lines; Fig. 3, E to G) with the aromatic ligand with similar distances (3.393, 3.317, and 3.346 Å for PX, MX, and OX, respectively), which suggests that this interaction may not be the dominant binding force. The distinct difference is found in the hydrogen bonds between the H atoms of the xylene methyl group and the O atoms from the ligand (site II, blue dotted lines; Fig. 3, E to G). There are four hydrogen bonds between PX and the 1D chain with distances in the range of 2.711 to 2.903 Å, whereas only three and two hydrogen bonds are formed between MX and OX and the chain because of the less-well-matched shape of the two molecules. The dipole-dipole interactions (site III,

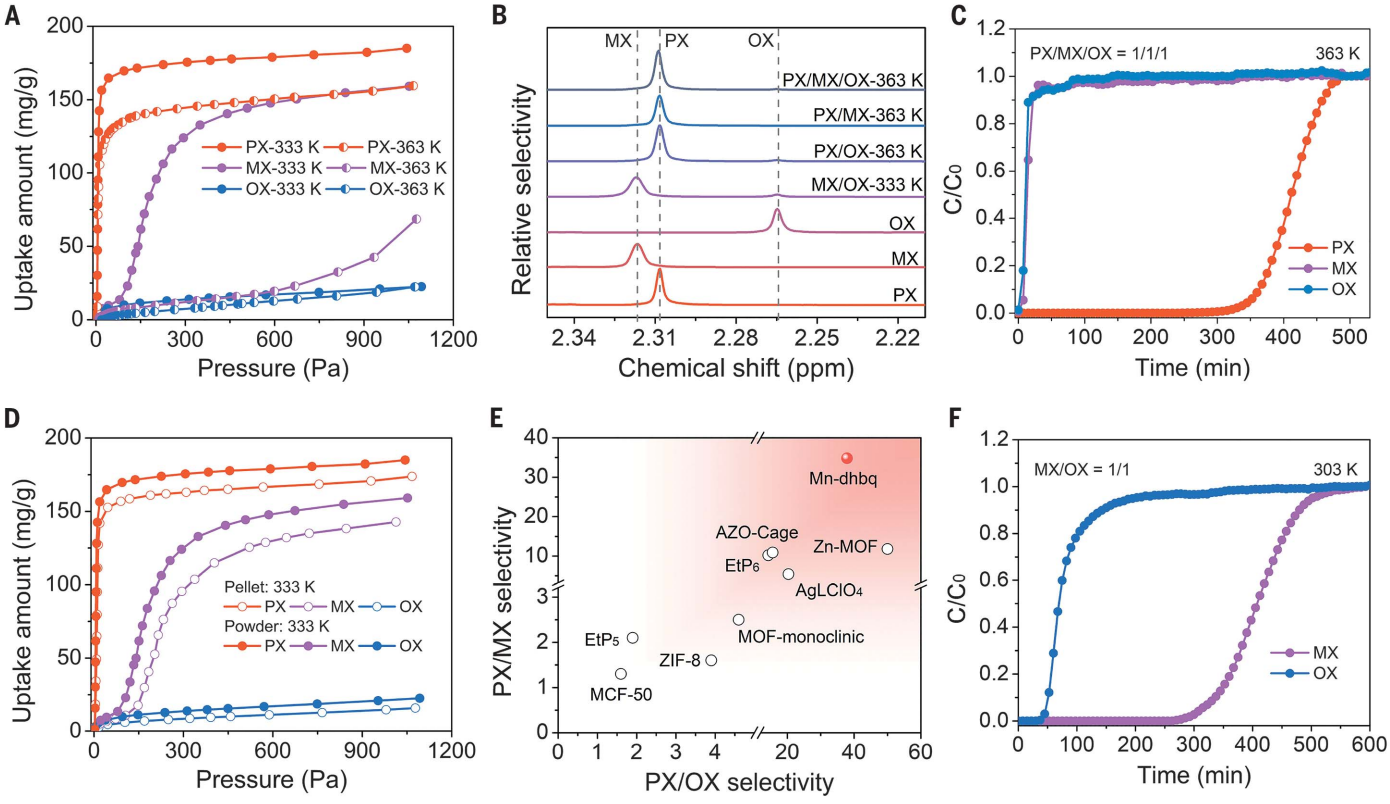

Fig. 2. Adsorption and separation of xylene isomers. (**A**) Single-component vapor adsorption isotherms of xylene isomers on Mn-dhbq at 333 and 363 K. (**B**) Magnified ^{1}H-NMR spectrum recorded using the $CDCl_3$ to extract xylene isomers from the decomposed Mn-dhbq by concentrated HCl solution that was priorly subjected to the equimolar binary or ternary vapor of xylene isomers at 333 and 363 K. ppm, parts per million. (**D**) The comparison of xylene vapor adsorption isotherms between Mn-dhbq powder and pellet samples at 333 K. (**E**) Comparison of adsorption selectivities for binary mixtures of PX/OX and PX/MX in vapor phase for Mn-dhbq and selected materials. For each reported material, only the highest and/or best values of selectivity were selected. (**C** and **F**) Breakthrough curves of an equimolar binary (F) and ternary (C) mixture of xylene isomers at 303 and 363 K for Mn-dhbq pellet samples. The partial pressure of xylenes in the feed gas used for binary and ternary breakthrough experiments is 2.4 and 3.9 kPa, respectively.

red dotted lines) between C_{methyl} and Mn^{2+} centers are also determined from molecular simulations (Fig. 3, E to G). For PX, there are two strong $C^{\delta-}\cdots Mn^{\delta+}$ dipole-dipole interactions between PX and the chain, with distances of 3.128 and 3.776 Å, respectively. For MX and OX, only one strong $C^{\delta-}\cdots Mn^{\delta+}$ dipole-dipole interaction exists (3.195 and 3.501 Å). The calculated binding energies of PX, MX, and OX (95.1, 92.8, and 87.1 kJ/mol) are fully consistent with the extent of three interactions and with the same descending order of the adsorption heats measured by differential scanning calorimeter (DSC) method (fig. S53). Additionally, thermogravimetric analysis of the xylene-loaded Mn-dhbq samples also confirmed the order of interactions (PX > MX > OX). The weakest-binding OX was lost from the sample at ~30°C, even though it has the highest boiling point among the three isomers. The weight loss of MX happened at ~95°C, followed by the loss of PX at ~126°C for MX- and PX-adsorbed Mn-dhbq (Fig. 3D and figs. S54 to S56). The relative binding strengths of the three xylene isomers correlate well with the observed phenomenon (*22*): PX is adsorbed at all experimental temperatures because its interaction with the Mn-dhbq framework is sufficiently strong to force the molecule to enter the constrained space at all temperatures. The intermediate binding energy between MX and Mn-dhbq is insufficient to allow the molecule to enter the voids at higher temperature (393 K). However, decreasing the temperature to a certain value (i.e., 363 K or below) will infuse sufficient energy to push MX into the adsorption sites. With the lowest binding energy, OX can only take up the sites at even lower temperatures (≤303 K).

Among reported sorbents for gas-vapor separations, many have poor chemical stability, especially those with open metal sites. By contrast, Mn-dhbq exhibits high resistance toward water, heat, and air over long periods of time, as confirmed by PXRD and porosity analysis (figs. S57 and S58). The porosity parameters of the activated Mn-dhbq sample remained nearly the same after being soaked in pure PX solution at 393 K for 24 hours or in boiled water for 1 week (fig. S58 and table S4). The in situ PXRD analysis on Mn-dhbq at various temperatures also points to its suitability for industrial xylene separations at relatively high temperatures, whereas Cu-metallocycle begins to show degradation at 433 K and loses crystallinity completely at 473 K (figs. S59 and S60). The PX uptake capacity (~147 mg/g) of Mn-dhbq remains unchanged after 20 consecutive adsorption-desorption cycles at 393 K (Fig. 4, A and B, and figs. S61 and S62). No obvious loss of PX uptake was observed after 10 consecutive adsorption cycles in the liquid phase at 393 K and subsequent desorption under nitrogen flow at 493 K (fig. S63). The Mn-dhbq structure remained intact with a stable cycling capacity of ~150 mg/g, whereas Cu-metallocycle lost its adsorption capacity and crystallinity after one cycle under identical conditions (figs. S63 and S64). The adsorbed PX was extracted from Mn-dhbq at 433 K (160°C, 1 hour), using 1,4-diethylbenzene (DEB) as desorbent, after adsorption of a quaternary liquid mixture of PX/OX/MX/EB (22/22/50/6) at 393 K (120°C). The purity of PX reached >97% with a recovery of 71% in a single desorption cycle (fig. S65). These results confirm the robustness and recyclability of Mn-dhbq. In

addition to the strong Mn-O bonds within the 1D chains, the flexible chain stacking structure that allows interchain rearrangement to quickly respond to the stimulus may be responsible for the reversible transformability between nonporous and porous states, leading to the high chemical stability of Mn-dhbq.

The commercially available raw chemicals and environmentally friendly method used to prepare Mn-dhbq are amenable for scaled-up synthesis. We achieved this by a simple one-pot reaction at room temperature using water as the only solvent. About 0.23 kg of Mn-dhbq was collected in a single batch (Fig. 4D) and formulated into pellets. The pellet sample exhibits high crystallinity (figs. S66 and S67) and similar separation performance as those of the powder samples (Fig. 2, C and F, and Fig. 4C).

A porous and robust coordination polymer, Mn-dhbq, having hydrogen-bonded 1D chains, multiple open-metal sites, rich π-electrons, and structural flexibility, can selectively recognize specific xylene isomers and is capable of full separation of OX, MX, and PX isomers through molecular sieving. Guest-induced structural rearrangement is important for the preferential interaction with specific xylene isomers. Two key properties of Mn-dhbq are the high separation selectivity for PX over MX and OX in both vapor and liquid phases, especially at higher temperatures, and the separation of all three xylene isomers in vapor phase through molecular sieving.

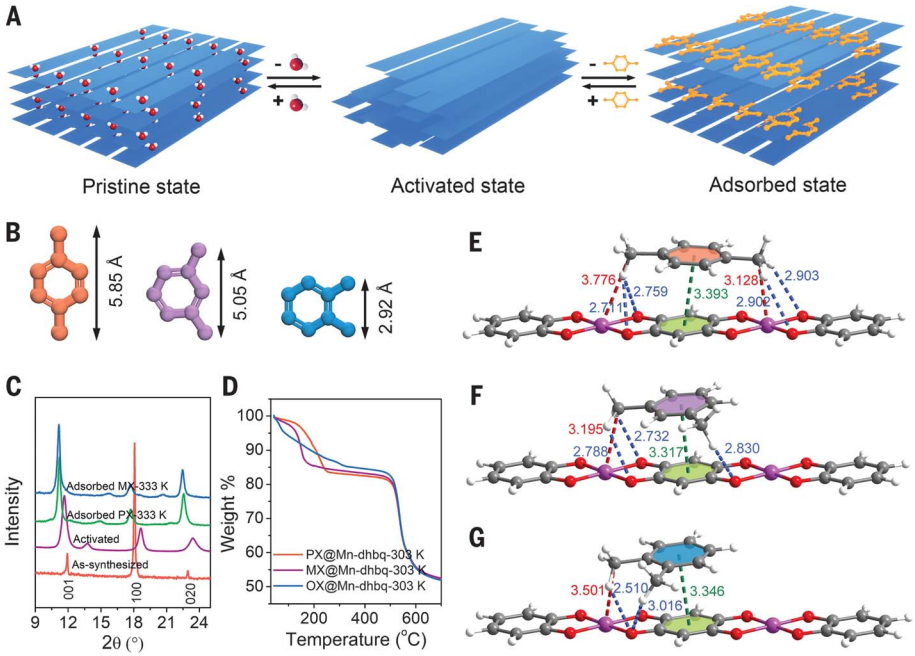

Fig. 3. Mechanism of framework swelling and xylene–Mn-dhbq interaction. (**A**) Schematic representations of the possible mechanism about the Mn-dhbq crystal structure changes corresponding with the stimulus. (**B**) The length between the two methyl groups for PX, MX, and OX molecules. (**C**) The comparison of PXRD patterns of as-synthesized, activated, and xylene-adsorbed Mn-dhbq samples. (**D**) The thermogravimetric (TG) curves of xylene@Mn-dhbq samples. (**E** to **G**) The adsorption binding sites, π-π stacking (site Is, green dotted lines), hydrogen bonds (site IIs, blue dotted lines), and $C_{methyl}^{\delta-}\cdots Mn(II)^{\delta+}$ dipole-dipole interactions (site IIIs, red dotted lines) between the xylene molecules and the 1D chain of the Mn-dhbq framework as determined by DFT simulations.

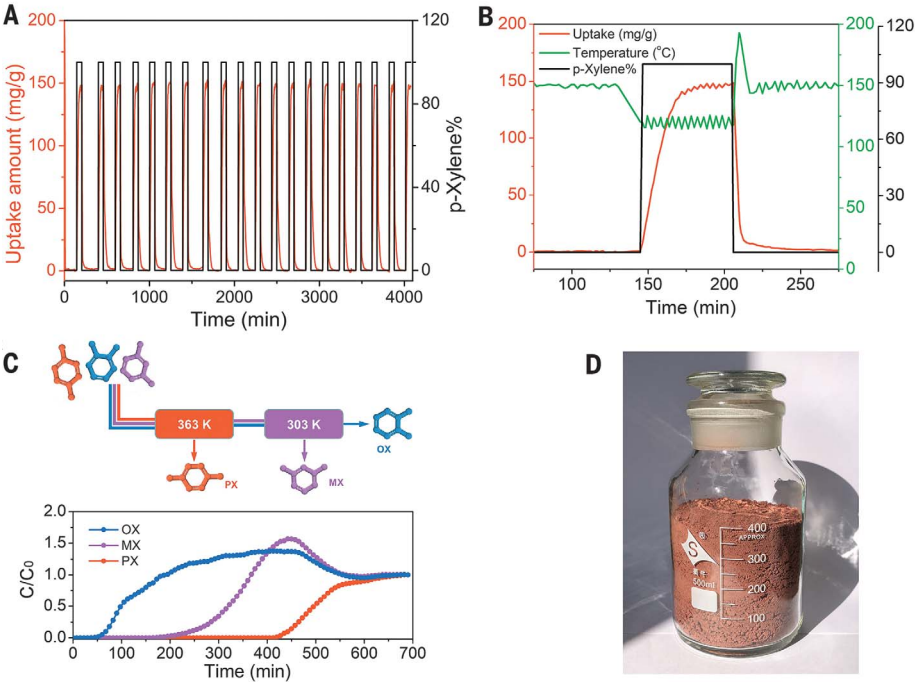

Fig. 4. Recyclability tests, breakthrough separation of xylene ternary mixture, and large-scale synthesis of Mn-dhbq. (**A**) The *p*-xylene adsorption-desorption recyclability test on Mn-dhbq powder samples for 20 consecutive adsorption cycles at 393 K. The orange and black curves indicate the uptake amount of *p*-xylene and the concentration of *p*-xylene combined with N_2 flow, respectively. (**B**) Enlarged image of the first cycle from (A) showing the *p*-xylene adsorption on Mn-dhbq at 393 K and desorption at 423 K under nitrogen flow. The green curve is the temperature of the adsorption chamber. (**C**) Breakthrough curves of an equimolar ternary mixture of all three xylenes (bottom) using Mn-dhbq pellets packed in two columns at 363 and 303 K (top). The partial pressure of xylenes in the feed gas used for the ternary breakthrough experiment is 3.9 kPa. (**D**) Scaled-up synthesis of as-synthesized Mn-dhbq obtained from rapid string and mixing of an aqueous solution of manganese acetate tetrahydrate and an aqueous solution of H_2dhbq ligand.

REFERENCES AND NOTES

1. M. Minceva, A. E. Rodrigues, *AIChE J.* **53**, 138–149 (2007).
2. G. Zhang, Y. Ding, A. Hashem, A. Fakim, N. M. Khashab, *Cell. Rep. Phys. Sci.* **2**, 100470 (2021).
3. D. S. Sholl, R. P. Lively, *Nature* **532**, 435–437 (2016).
4. Y. Yang, P. Bai, X. Guo, *Ind. Eng. Chem. Res.* **56**, 14725–14753 (2017).
5. L. S. Cheng, J. A. Johnson, "Adsorbents with improved mass transfer properties and their use in the adsorptive separation of para-xylene," US Patent 8,609,925 (2013).
6. B. Van de Voorde, B. Bueken, J. Denayer, D. De Vos, *Chem. Soc. Rev.* **43**, 5766–5788 (2014).
7. G.-Q. Guo, H. Chen, Y.-C. Long, *Microporous Mesoporous Mater.* **39**, 149–161 (2000).
8. K. Jie *et al*., *J. Am. Chem. Soc.* **140**, 6921–6930 (2018).
9. N. Sun *et al*., *Chem. Sci.* **10**, 8850–8854 (2019).
10. G. W. Zhang *et al*., *Chem* **6**, 1082–1096 (2020).
11. M. Lusi, L. J. Barbour, *Angew. Chem. Int. Ed.* **51**, 3928–3931 (2012).
12. M. du Plessis, V. I. Nikolayenko, L. J. Barbour, *J. Am. Chem. Soc.* **142**, 4529–4533 (2020).
13. B. Moosa *et al*., *Angew. Chem. Int. Ed.* **59**, 21367–21371 (2020).
14. M. I. Gonzalez *et al*., *J. Am. Chem. Soc.* **140**, 3412–3422 (2018).
15. V. Finsy *et al*., *J. Am. Chem. Soc.* **130**, 7110–7118 (2008).
16. A. Torres-Knoop, R. Krishna, D. Dubbeldam, *Angew. Chem. Int. Ed.* **53**, 7774–7778 (2014).
17. X. Li *et al*., *Nat. Commun.* **11**, 4280 (2020).
18. J. M. Holcroft *et al*., *J. Am. Chem. Soc.* **137**, 5706–5719 (2015).
19. L. Alaerts *et al*., *Angew. Chem. Int. Ed.* **46**, 4293–4297 (2007).
20. L. Yang *et al*., *ACS Appl. Mater. Interfaces* **13**, 41600–41608 (2021).
21. D. D. Zhou *et al*., *Nat. Mater.* **18**, 994–998 (2019).
22. H. Wang *et al*., *Energy Environ. Sci.* **11**, 1226–1231 (2018).
23. P. J. Bereciartua *et al*., *Science* **358**, 1068–1071 (2017).
24. C. Gu *et al*., *Science* **363**, 387–391 (2019).
25. L. Alaerts *et al*., *J. Am. Chem. Soc.* **130**, 14170–14178 (2008).
26. S. Q. Wang *et al*., *Angew. Chem. Int. Ed.* **58**, 6630–6634 (2019).
27. S. Mukherjee *et al*., *Sci. Rep.* **4**, 5761 (2014).
28. X. Cui *et al*., *Nat. Commun.* **11**, 5456 (2020).
29. S. Morikawa, T. Yamada, H. Kitagawa, *Chem. Lett.* **38**, 654–655 (2009).
30. T. Yamada, S. Morikawa, H. Kitagawa, *Bull. Chem. Soc. Jpn.* **83**, 42–48 (2010).
31. R. W. Neuzil, "Aromatic hydrocarbon separation by adsorption," US Patent 3,558,730 (1971).
32. D. M. Polyukhov, A. S. Poryvaev, A. S. Sukhikh, S. A. Gromilov, M. V. Fedin, *ACS Appl. Mater. Interfaces* **13**, 40830–40836 (2021).
33. J. Crank, *The Mathematics of Diffusion* (Oxford Univ. Press, 1975).
34. M. Minceva, A. E. Rodrigues, *Chem. Eng. Res. Des.* **82**, 667–681 (2004).

ACKNOWLEDGMENTS

We thank Y. Liu and J. D. Hu for their help in the graphic work in Fig. 3. **Funding:** This work was supported by the National Natural Science Foundation of China (21722609, 21878260, and 22141001) and the Zhejiang Provincial Natural Science Foundation of China (LR170B060001). The Rutgers team thanks the US Department of Energy for the partial support through grant DE-SC0019902. **Author contributions:** Z.B. and J.L. conceived and designed the project. L.L. synthesized the materials, performed most of the vapor adsorption and breakthrough experiments, and drafted the manuscript. L.G. carried out the molecular simulation and analyzed the binding sites of the guests. D.H.O. collected and analyzed the kinetic adsorption data. S.X. conducted sorption cycling tests. K.W. prepared the shaped pellets for the vapor adsorption isotherms. Z.Z., Q.Y., and Y.Y. discussed the experimental results and gave valuable suggestions. J.L. and Q.R. supervised the experiment and revised the manuscript. **Competing interests:** The authors declare no competing interests. **Data and materials availability:** All data are available in the main text or the supplementary materials.

SUPPLEMENTARY MATERIALS

science.org/doi/10.1126/science.abj7659
Materials and Methods
Figs. S1 to S67
Tables S1 to S6
References (*35*–*60*)
Data S1

Submitted 31 May 2021; resubmitted 12 April 2022
Accepted 15 June 2022
10.1126/science.abj7659

Science

Discrimination of xylene isomers in a stacked coordination polymer

Liangying LiLidong GuoDavid H. OlsonShikai XianZhiguo ZhangQiwei YangKaiyi WuYiwen YangZongbi BaoQilong RenJing Li

Science, 377 (6603), • DOI: 10.1126/science.abj7659

Using polymers to separate xylene isomers

Each of the three xylene isomers is a valuable feedstock for many chemical processes. However, because they have similar boiling points, separation by distillation or other evaporative methods is energy intensive and inefficient. Li *et al*. developed an alternative separation process using a manganese-based, stacked, one-dimensional coordination polymer with an interchain distance that varies with temperature and the content of the adsorbed hydrocarbons. At 393 kelvin, only *p*-xylene can access the voids, whereas *m*-xylene can enter at temperatures between 333 and 393 kelvin and *o*-xylene only below 333 kelvin. Through a sequence of separations, each isomer can be extracted with high selectivity. The material is simple, cost-effective, and easily scalable, and it exhibits remarkable water and air stability and excellent recyclability. —MSL

Science (ISSN) is published by the American Association for the Advancement of Science. 1200 New York Avenue NW, Washington, DC 20005. The title *Science* is a registered trademark of AAAS.